Characterization of the Structure of the Anthramycin-d(ATGCAT)$_2$ Adduct by NMR and Molecular Modeling Studies. Determination of the Stereochemistry of the Covalent Linkage Site, Orientation in the Minor Groove of DNA, and Effect on Local DNA Structure

F. Leslie Boyd,[†] Steven F. Cheatham,[†] William Remers,[‡] G. Craig Hill,[‡] and Laurence H. Hurley*,[†]

Contribution from the Division of Medicinal and Natural Products Chemistry, College of Pharmacy, University of Texas at Austin, Austin, Texas 78712, and Department of Medicinal Chemistry, College of Pharmacy, University of Arizona, Tucson, Arizona 85721.
Received May 2, 1988

Abstract: Anthramycin is a member of the pyrrolo[1,4]benzodiazepine group of antitumor antibiotics. Previous studies have demonstrated that anthramycin binds covalently through N-2 of guanine within the minor groove of DNA, resulting in a relatively nondistortive DNA adduct. From the nuclear Overhauser effect spectroscopy (NOESY) proton NMR spectra of the anthramycin-d(ATGCAT)$_2$ adduct, we have obtained results that unambiguously assign the orientation of the drug molecule in the minor groove of DNA. Four sets of NOE cross-peaks between anthramycin protons and nucleotide protons on either the covalently or the noncovalently modified strands reveal that the drug is specifically oriented with the aromatic ring to the 3′-side of the covalently modified guanine. Unequivocal assignment of the geometry at the site of attachment of anthramycin to d(ATGCAT)$_2$ cannot be made by *J*-correlated spectroscopy (COSY). However, when combined with the results of modeling with the molecular mechanics program AMBER, an 11*S* stereochemistry at this site can be confidently predicted. ^{31}P NMR studies show that two of the resonance signals in the anthramycin-d(ATGCAT)$_2$ adduct have moved significantly downfield. Both downfield ^{31}P NMR signals have been assigned by ^{17}O isotopic labeling and ^{1}H-^{31}P two-dimensional *J*-correlation experiments and shown to correspond to the phosphates on the 5′-sides of the covalently modified deoxyguanine and the deoxycytosine on the opposite strand. Assignment of resonance signals of nonexchangeable base and sugar protons of the anthramycin-d(ATGCAT)$_2$ has been made with two-dimensional Fourier transform NMR methods (COSY and NOESY). Conformational details about the sugar puckers, the glycosidic dihedral angles, and the effect of anthramycin bonding on secondary structure of the duplex have been obtained from the relative intensities of cross-peaks in the two-dimensional NMR spectra in aqueous solution. All of the sugars that are amenable to this analysis possess a conformation consistent with B-type DNA. Molecular mechanics calculations with AMBER are predictive of the orientation and stereochemistry of anthramycin bound to d(ATGCAT)$_2$. The species having an 11*S* stereochemistry at the covalent bonding site and oriented with the aromatic ring of anthramycin to the 3′-side of the covalently modified guanine of anthramycin-d(ATGCAT)$_2$ appears to be favored over the three other possible species. This is because of the greater intermolecular binding for this species rather than lower helix distortion energies. The molecular modeling is also in accord with the experimentally determined nondistortive nature of the anthramycin-d(ATGCAT)$_2$ adduct.

Anthramycin (Figure 1) is the lead member of the naturally occurring pyrrolo[1,4]benzodiazepine (P[1,4]B) antitumor antibiotics.[1] This potent antitumor compound is produced by *Streptomyces refuineus*,[2] and its biosynthetic origin[3] and total synthesis[4] have been reported. The cytotoxic and antitumor effects of anthramycin and related compounds are believed to be due to their selective interaction with DNA,[5] which causes inhibition of nucleic acid synthesis,[6] and production of excision-dependent single- and double-strand breaks in cellular DNA.[7] Studies from this laboratory[8] and others[5] have provided strong evidence that C11 of anthramycin reacts selectively with the N-2 of guanine in duplex DNA to form an aminal linkage (Figure 2). Further evidence for the covalent linkage sites between anthramycin and DNA has been provided through ^{1}H and ^{13}C NMR experiments on 6-*mer*- and 140-*mer*-anthramycin-DNA adducts, respectively.[9] Proton NMR and fluorescence measurements on tomaymycin (Figure 1), another P[1,4]B antibiotic, suggest that the N10,C11 imine is the DNA-reactive species[10] (Figure 2). DNA footprinting studies and an exonuclease III stop assay have shown that anthramycin prefers to bond to 5′-PuGPu sequences, while 5′-PuGPy and 5′-PyGPu are of intermediate preference and 5′-PyGPy sequences are least favored.[11,12] Molecular modeling studies on the anthramycin-DNA adduct have been carried out by three different groups.[13-15] A combined NMR, fluorescence, and molecular modeling study shows that tomaymycin bonds to d(ATGCAT)$_2$ in two orientations, each having opposite linkage

* To whom correspondence should be addressed.
[†] University of Texas at Austin.
[‡] University of Arizona.

(1) For reviews on the P[1,4]B antitumor antibiotics, see the following. For pharmacological and toxicological aspects: Hurley, L. H. *J. Antibiot.* **1977**, *30*, 349. For mechanism of action studies: Hurley, L. H.; Needham-VanDevanter, D. R. *Acc. Chem. Res.* **1986**, *19*, 230. For synthesis and mechanism of action studies see: Remers, W. A. In *The Chemistry of Antitumor Antibiotics*; John Wiley & Sons: New York, 1988; Vol. 2, pp 28-92.
(2) Tendler, M. D.; Korman, S. *Nature (London)* **1963**, *199*, 501.
(3) Hurley, L. H. *Acc. Chem. Res.* **1980**, *13*, 263.
(4) Leimgruber, W.; Batcho, A. D.; Czajkowski, R. C. *J. Am. Chem. Soc.* **1968**, *90*, 5641.
(5) (a) Kohn, K. W.; Glaubiger, D.; Spears, C. L. *Biochem. Biophys. Acta* **1974**, *361*, 288. (b) Hurley, L. H.; Gariola, C.; Zmijewski, M. *Biochem. Biophys. Acta* **1977**, *475*, 521.
(6) Kohn, K. W. Anthramycin. In *Antibiotics III. Mechanism of Action of Antimicrobial and Antitumor Agents*; Corcoran, J. W., Hahn, F. E., Eds.; Springer-Verlag: New York, 1975; pp 3-11.
(7) Petrusek, R. L. D.; Uhlenhopp, E. L.; Duteau, N.; Hurley, L. H. *J. Biol. Chem.* **1982**, *257*, 6207.
(8) Petrusek, R. L.; Anderson, G. L.; Garner, T. F.; Fannin, Q. L.; Kaplan, D. J.; Zimmer, S. G.; Hurley, L. H. *Biochemistry* **1981**, *20*, 1111.
(9) Graves, D. E.; Pattaroni, C.; Balakrishnan, C.; Ostrander, J. M.; Hurley, L. H.; Krugh, T. R. *J. Biol. Chem.* **1984**, *259*, 8202.
(10) Barkley, M.; Cheatham, S.; Thurston, D. E.; Hurley, L. H. *Biochemistry* **1986**, *103*, 7629.
(11) Hertzberg, R. P.; Hecht, S. M.; Reynolds, V. L.; Molineaux, I. J.; Hurley, L. H. *Biochemistry* **1986**, *25*, 1249.
(12) Hurley, L. H.; Reck, T.; Thurston, D. E.; Holden, K. G.; Hertzberg, R. P.; Hoover, J. R. E.; Gallagher, G., Jr.; Faucette, L. F.; Mong, S. M.; Johnson, R. K. *Chem. Res. Toxicol.* **1988**, *1*, 258.
(13) Zakrzewska, K.; Pullman, B. *J. Biomol. Struct. Dyn.* **1986**, *4*, 127.

0002-7863/90/1512-3279$02.50/0

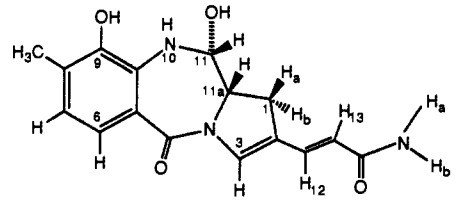

Anthramycin

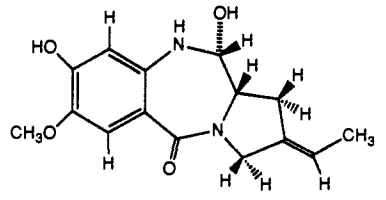

Tomaymycin

Figure 1. Structures of anthramycin and tomaymycin.

stereochemistries.[16] More recently, tomaymycin has been shown to covalently bond through N-2 of guanine in the sequence 5′-CGA with an 11*S* stereochemistry and 3′-orientation of the aromatic ring relative to the covalently modified guanine.[17] A previous one- and two-dimensional ^{1}H NMR study on anthramycin–d(ATGCAT)$_2$ has appeared.[18] This present study extends the previous one in several important respects. The orientation of anthramycin on d(ATGCAT)$_2$, as tentatively defined in a previous study,[18] is now confirmed. A combined two-dimensional NOESY and molecular modeling approach provides convincing evidence for the stereochemistry at the covalent linkage site. Conformational aspects of the drug-modified duplex are examined by two-dimensional ^{1}H and ^{31}P NMR spectroscopy. Molecular modeling with AMBER is used to provide additional insight into binding interactions that stabilize the species of anthramycin–d(ATGCAT)$_2$ found in solution. A preliminary account of this work has appeared.[19]

Results and Discussion

Although the positions of the covalent linkage sites between anthramycin and DNA have been accepted for some time,[8] the stereochemistry of the aminal linkage at C11 and orientation of the drug molecule in the minor groove have yet to be firmly established.[18] In the earlier published work from this laboratory, Corey–Pauling–Koltum (CPK) models were used to predict the linkage geometry and orientation of anthramycin in the minor groove of DNA.[8] In these studies, and in subsequent publications, an 11*S* stereochemistry at the covalent linkage site with the aromatic ring to the 3′-side of the covalently modified guanine (**A** in Figure 3) was assumed, but without definite experimental data. The orientation of the aromatic ring of anthramycin to the 3′-side of the covalently modified guanine was seemingly confirmed in a more recent two-dimensional ^{1}H NMR study,[18a] but we are unable to reproduce the results of this particular experiment (see later text). In addition, this study provided only limited information on the effect of drug bonding on local DNA structure. Theoretical modeling studies have also been recently published[13-14] that address the important questions of the stereochemistry at the covalent linkage site in the self-complementary duplex d(ATGCAT)$_2$ and the effect of drug bonding on local DNA structure.

In view of the importance of these assignments for future work designed to determine the effect of variation of drug structure and sequence on P[1,4]B bonding to DNA, we have undertaken a combined molecular modeling and one- and two-dimensional ^{31}P and ^{1}H NMR analysis designed to remove these uncertainties. The combined modeling and NMR approach also permits the predictability of modeling with the molecular mechanics program AMBER to be evaluated for drug–DNA adduct systems. Although the 6-*mer* self-complementary duplex chosen for this study belongs to the 5′-PyGPy class, and is therefore not a favored sequence for P[1,4]B binding.[11-12] the previous ^{1}H NMR studies[9,18] on this oligomer led us to use this self-complementary oligomer. In principle, there are the four possible anthramycin–d(ATGCAT)$_2$ adduct species, as shown in Figure 3. Consequently, an additional complication might be the presence of more than one species of the anthramycin–duplex adduct, e.g., a mixture of species **A** and **B** in Figure 3. In this respect, in a previous combined fluorescence, ^{1}H NMR, and molecular modeling study on tomaymycin bound to d(ATGCAT)$_2$, we have confirmed that this drug may bond with either the 11*S* or 11*R* linkage geometry and most likely, as species equivalent to **A** and **D** shown in Figure 3.[16] However, in the more preferred bonding sequence 5′-CGA, contained in a self-complementary 12-*mer*, there is only one species of tomaymycin covalently bound (i.e., that having an 11*S* linkage stereochemistry and 3′-orientation, equivalent to species **A** in Figure 3).[17]

Determination of the Number of Species of Anthramycin Bound Covalently to d(ATGCAT)$_2$ by ^{31}P and ^{1}H NMR. Anthramycin–d(ATGCAT)$_2$ adducts were prepared by adding excess drug to a d(ATGCAT) solution that was stirred for 4 days at 4 °C before removal of excess anthramycin. The solution structure of the anthramycin–d(ATGCAT)$_2$ adduct was observed at 500 MHz in sodium acetate and sodium phosphate buffered D_2O, which was degassed with argon at 23 °C.

The complexity of the anthramycin–d(ATGCAT)$_2$ adduct relative to d(ATGCAT), which exists as an equilibrium between double- and single-stranded forms at 23 °C, was examined by both one-dimensional and two-dimensional ^{1}H and ^{31}P NMR experiments. In the oligomer d(ATGCAT) just five phosphorus signals are observed (Figure 4A). However, upon formation of the anthramycin–d(ATGCAT)$_2$ adduct, twice the number of phosphorus signals are seen (Figure 4B). This is in accord with the loss of duplex symmetry due to formation of just one species of duplex adduct. Two of the ten phosphorus signals are moved significantly downfield upon adduct formation. These have been assigned to individual phosphates by two-dimensional ^{31}P–^{1}H *J*-correlation NMR experiments (see later text).

The two-dimensional COSY spectrum of the anthramycin–d(ATGCAT)$_2$ adduct is not shown in Figure 5. In comparison to d(ATGCAT) alone[20] and the tomaymycin–d(ATGCAT)$_2$ adduct,[16] the spectrum of the anthramycin–duplex adduct is of intermediate complexity. The assignments of the chemical shifts for the aromatic base protons and 1′-, 2′-, 2″- and 3′-deoxyribose protons for the d(ATGCAT) and the anthramycin–d(ATGCAT)$_2$ adduct, together with their chemical shifts changes upon adduct formation, are shown in Table IA,B. Likewise, the anthramycin and anthramycin–adduct proton assignments and chemical shift changes are shown in Table II. Twice the number of DNA proton resonance signals appear in the anthramycin–d(ATGCAT)$_2$ adduct in comparison to the duplex alone. Just as for the ^{31}P NMR spectra, this is in accord with the loss of duplex symmetry due to formation of just one species of the anthramycin–d(ATGCAT)$_2$ adduct. Furthermore, only one set of anthramycin ^{1}H resonances appears in the spectrum of the anthramycin–d(ATGCAT)$_2$ adduct

(14) Remers, W. A.; Mabilia, M.; Hopfinger, A. J. *J. Med. Chem.* **1986**, *29*, 2492.
(15) Rao, S. N.; Singh, U. C.; Kollman, P. A. *J. Med. Chem.* **1986**, *29*, 2484.
(16) Cheatham, S.; Kook, A.; Hurley, L. H.; Barkley, M.; Remers, W. *J. Med. Chem.* **1988**, *31*, 583.
(17) Boyd, F. L.; Stewart, D.; Remers, W. A.; Barkley, M. D.; Hurley, L. H. *Biochemistry* **1990**, *29*, 2387.
(18) (a) Graves, D. E.; Stone, M. P.; Krugh, T. R. *Biochemistry* **1985**, *24*, 7573. (b) In a more recent contribution that was submitted for publication while this manuscript was in review Krugh and co-workers have provided additional data that confirm their preliminary findings and there is agreement with the data presented here. Krugh, T. R.; Graves, D. E.; Stone, M. P. *Biochemistry* **1989**, *28*, 9988.
(19) Boyd, F. L.; Cheatham, S.; Hurley, L. H. *Abstracts of Papers*, 193rd American Chemical Society Meeting, Denver, CO, 1987; American Chemical Society: Washington, DC, 1987; MEDI 049.
(20) Patel, D. J.; Tonelli, A. E. *Biochemistry* **1975**, *14*, 3990.

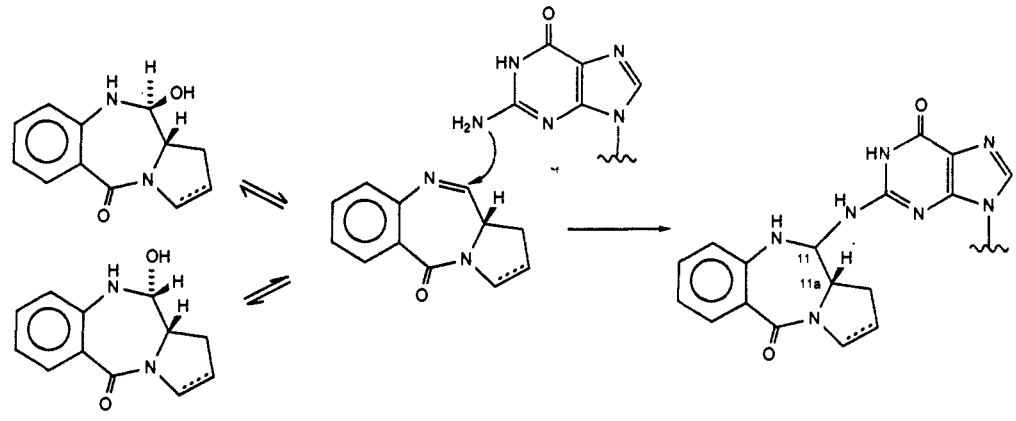

Figure 2. Proposed mechanism for alkylation of DNA by the N10,C11 imine to form the P[1,4]B–N-2-guanine—DNA adduct.[10]

Table I

A. Comparison of the Base Proton Chemical Shift Assignments (ppm) and T_1 Relaxation Times of Nonexchangeable Protons of d(ATGCAT)$_2$ and Anthramycin-d(ATGCAT)$_2$ Adduct in D_2O at 24 °C

	d(ATGCAT)	anthramycin-d(ATGCAT)$_2$			d(ATGCAT)	anthramycin-d(ATGCAT)$_2$	
assgnt	δ	δ	Δ	assgnt	δ	δ	Δ
^{1}AH8	8.09	8.10	+0.01	^{1}AH2	7.87 (4.72)[i]	7.98 (4.96)[i]	+0.21 (0.24)
^{2}TH6	7.29	7.36	+0.07	^{2}TMe	1.46	1.45	−0.01
^{3}GH8	7.86	7.87	+0.01	^{4}CH5	5.37	5.43	+0.06
^{4}CH6	7.32	7.39	+0.07	^{5}AH2	7.81 (5.13)[i]	8.00 (5.25)[i]	+0.19 (0.12)
^{5}AH8	8.26	8.16	−0.10	^{6}TMe	1.29	1.35	+0.06
^{6}TH6	7.23	7.17	−0.06	^{7}AH2	7.87 (4.72)[i]	7.96 (5.46)[i]	+0.09 (0.26)
^{7}AH6	8.09	8.21	+0.12	^{8}TMe	1.46	1.41	−0.05
^{8}TH6	7.29	7.26	−0.03	^{10}CH5	5.37	5.57	+0.20
^{9}GH8	7.86	7.88	+0.02	^{11}AH2	7.81 (5.13)[i]	7.70 (3.38)[i]	−0.11 (1.75)
^{10}CH6	7.32	7.45	+0.13	^{12}TMe	1.29	1.33	+0.04
^{11}AH8	8.26	8.30	+0.04				
^{12}TH6	7.23	7.16	−0.07				

B. Comparison of the Deoxyribofuranose Proton Chemical Shift Assignments (ppm) of d(ATGCAT) and the Anthramycin-d(ATGCAT)$_2$ Adduct

	H1′			H2′			H2″			H3′		
assign	6-*mer*	Anth-6-*mer*	Δδ[a]	6-*mer*	Anth-6-*mer*	Δδ[a]	6-*mer*	Anth-6-*mer*	Δδ[a]	6-*mer*	Anth-6-*mer*	Δδ[a]
^{1}A	6.14	6.25	+0.09	2.61[b]	2.65	+0.04	2.78	2.96	+0.18	4.85	4.88[e]	+0.07
^{2}T	5.71	5.54	−0.17	2.15[c]	2.31	+0.16	2.42	2.47[f]	+0.04	4.85	4.88[e]	+0.03
^{3}G	5.88	6.03	+0.15	2.61[b]	2.47[f]	−0.14	2.70[d]	2.77	+0.07	4.97	4.96	−0.01
^{4}C	5.68	5.78	+0.10	1.95	2.15[g]	+0.20	2.35	2.47[f]	+0.12	4.85	4.88[e]	+0.03
^{5}A	6.26	6.12	−0.14	2.70[d]	2.47[f]	−0.23	2.86	2.83	−0.03	4.97[h]	4.76	−0.23
^{6}T	6.08	6.16	+0.08	2.15[c]	2.15[g]	0.00	2.15[c]	2.15[g]	0.00	4.85	4.50	−0.35
^{7}A	6.14	6.21	+0.07	2.61	2.65	+0.04	2.78	2.87	+0.09	4.85	4.88[e]	+0.03
^{8}T	5.71	5.68	−0.03	2.14	2.15[g]	0.01	2.42	2.47[f]	+0.03	4.85	4.88[e]	+0.03
^{9}G	5.88	5.61	−0.27	2.61	2.67	+0.06	2.70	2.47[f]	−0.23	4.97	4.95	−0.02
^{10}C	5.68	6.03	+0.35	1.95	2.04	+0.09	2.35	2.47[f]	+0.12	4.85	4.88[e]	+0.02
^{11}A	6.26	5.99	−0.27	2.70	2.65	−0.05	2.86	2.65	−0.21	4.97	4.79	−0.18
^{12}T	6.08	6.07	−0.01	2.15	2.15[g]	0.00	2.15	2.15[g]	0.00	4.85	4.55	−0.30

[a] Δδ underlined are >±0.20. [b] δ 2.65–2.57 ^{1}AH2′ further downfield than ^{3}GH2′. [c] Overlapping chemical shifts in the range δ 2.21–2.08—order downfield to upfield ^{6}TH2″, ^{6}TH2′, ^{2}TH2′. [d] δ 2.75–2.66 ^{5}AH2′ further downfield than ^{3}GH2″. [e] Overlapping chemical shifts in the range δ 4.92–4.83—order downfield to upfield ^{8}TH3′, ^{4}CH3′, ^{2}TH3′, ^{1}AH3′, ^{7}AH3′, ^{10}CH$_3$—confirmed by H8/H6-H3′ cross-peaks in two-dimensional NOESY and H2′-H3′ cross-peaks in two-dimensional COSY. [f] Overlapping chemical shifts in the range δ 2.51–2.42—order downfield to upfield ^{5}AH2, ^{3}GH2′, ^{2}TH2″ ≈ ^{4}CH2″ ≈ 8TH2″ ≈ 9GH2″ ≈ ^{10}CH2″. [g] Overlapping chemical shifts in the range δ 2.21–2.09—order downfield to upfield ^{6}TH2″, ^{6}TH2′, ^{4}CH2′, ^{8}TH2′, ^{12}TH2″, H2′. [h] Under HOD peak. [i] T_1 values are given in seconds.

Table II. Comparison of the Proton Chemical Shift (ppm) Assignments in Anthramycin Alone and in the Anthramycin-d(ATGCAT)$_2$ Adduct[a]

species[b]	H1	H3	H6	$J_{6,7}$ (Hz)	H7	8-CH$_3$	H11	$J_{11,11a}$ (Hz)	H11a	H12	$J_{12,13}$ (Hz)	H13
ANTH	3.12	7.24	7.81 (d)[c]	8.34	6.89 (d)	2.18	4.99 (d)	8.91	3.81 (dd)[c]	7.35 (d)	15.8	5.87 (d)
ANTH-d(ATGCAT)$_2$	3.80	7.60	7.26 (d)[c]	8.23	6.90 (d)	2.41	6.03		4.45	7.62 (d)	23	6.25 (d)
adduct	3.50											
Δδ	+0.68											
	+0.38	+0.36	−0.55		+0.01	+0.23	+1.04		+0.64	+0.27		+0.38

[a] For numbering of anthramycin, see Figure 1. [b] Chemical shifts are in δ with TSP as an internal reference. [c] Key: d = doublet, dd = doublet of doublets.

(see Figure 5 and Table II), in contrast to the two sets of tomaymycin signals found in the spectrum of the tomaymycin–d-(ATGCAT)$_2$ adducts.[16] Last, the two-dimensional COSY spectrum (Figure 5) shows two intense sets of cytosine H5–H6 cross-peaks and four sets of thymine H5–C6CH$_3$ cross-peaks, confirming the loss of duplex symmetry with formation of a single species of the anthramycin-d(ATGCAT)$_2$ adduct. While these results are more complete than those previously reported,[18a] there

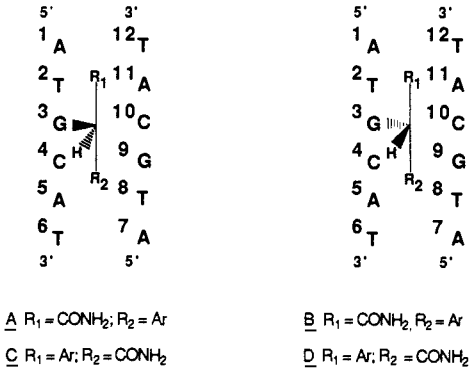

Figure 3. Schematic representations of the possible C11-enantiomeric N-2-guanine–d(ATGCAT)$_2$ adducts: **A**, 11*S* aromatic ring to the 3′-side; **B**, 11*R* aromatic ring to the 3′-side; **C**, 11*S* aromatic ring to the 5′-side; **D**, 11*R* aromatic ring to the 5′-side.

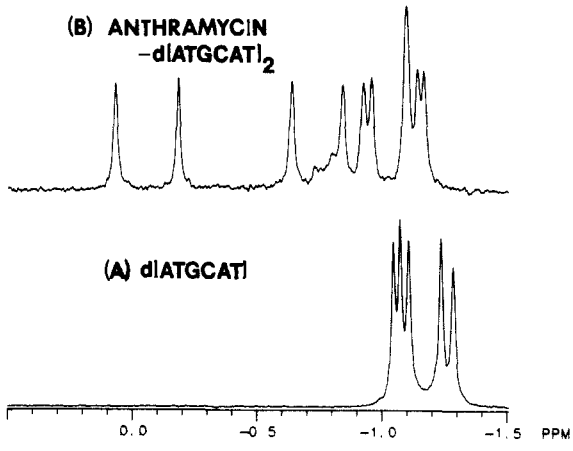

Figure 4. One-dimensional ^{31}P NMR spectra of the d(ATGCAT) (A) and the anthramycin–d(ATGCAT)$_2$ adduct (**B**).

is complete accord between these two reports.

Chemical Shift Changes of Nonexchangeable Protons Occurring on Bonding of Anthramycin to d(ATGCAT)$_2$. A comparison of the chemical shifts of protons in d(ATGCAT) and anthramycin with the anthramycin–d(ATGCAT)$_2$ adduct is shown in Tables IA,B and II. Only minor changes in the base aromatic proton chemical shifts occur in the anthramycin–d(ATGCAT)$_2$ adduct. However, for the adenine H_2 protons, the ^{11}A proton moves upfield by 0.11 ppm in contrast to the downfield shifts of ^{1}A, ^{5}A, and ^{7}A protons. The proximity of $^{11}AH_2$ to the acrylamide side chain of anthramycin is probably responsible for this effect. The most significant chemical shift changes for deoxyribose protons occurs for H1′ protons (^{9}G, ^{10}C, and ^{11}A), H2′ protons (^{4}C and ^{5}A), and H2″ protons (^{9}G and ^{11}A). The majority of these protons are also in proximity to anthramycin, and these changes may be rationalized by (de)shielding effects. Downfield shifts of anthramycin protons resulting from bonding to d(ATGCAT)$_2$ occur for H1a, H1b, H3, 8-CH_3, H11, H11a, H12, and H13, and these are particularly pronounced for H11 and H11a. The H6 proton of anthramycin shifts upfield.

Determination of the Orientation of the Anthramycin Molecule in the Minor Groove of d(ATGCAT)$_2$ by Two-Dimensional ^{1}H NMR. In principle, species **A** and **B** in Figure 3 can be differentiated from species **C** and **D** if unambiguous through-space interproton connectivities between anthramycin and d(ATGCAT)$_2$ protons can be identified. Examination of molecular models of species **A**–**D** of anthramycin–d(ATGCAT)$_2$ adducts shows that the H_2 proton of adenine-11 ($^{11}AH_2$) is in proximity to either the anthramycin side chain H13 proton in **A** and **B** or the aromatic 8-CH_3 protons in **C** and **D** of Figure 3, respectively. Therefore, identification of a NOE cross-peak between either anthramycin H13 or 8-CH_3 proton and the $^{11}AH_2$ proton would distinguish between the pairs **AB** or **CD**. Figure 6 shows an expansion of part of the two-dimensional NOESY ^{1}H NMR spectrum of the anthramycin–d(ATGCAT)$_2$ adduct at a mixing time of 250 ms. A cross-peak (A) is evident between anthramycin H13 and an adenine H_2 previously assigned as that due to ^{11}A.[16] A through-space connectivity (B in Figure 6) between the anthramycin protons at

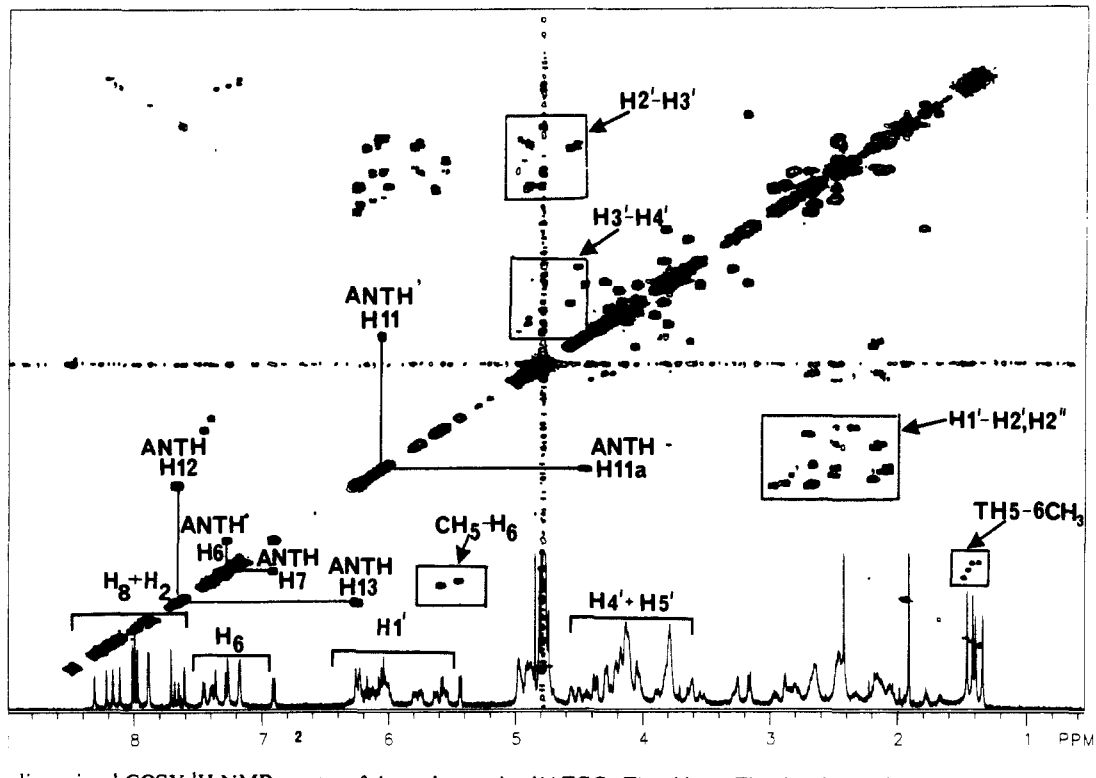

Figure 5. Two-dimensional COSY ^{1}H NMR spectra of the anthramycin–d(ATGCAT)$_2$ adduct. The chemical shift regions for the oligodeoxynucleotide aromatic and sugar protons are bracketed or correspond to the enclosed boxes for the H2′, H2″, and thymine methyl protons. Scalar coupling between anthramycin protons is indicated by the vertical and horizontal lines. An expanded spectrum of the H1′ to H2′ and H2″ region is shown in Figure 10.

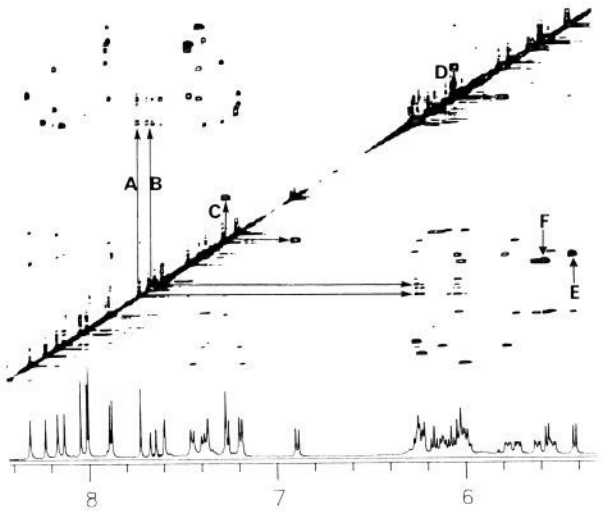

Figure 6. Expansion of part of the two-dimensional NOESY ^{1}H NMR spectrum of the anthramycin–d(ATGCAT)$_2$ adduct at a mixing time of 250 ms. The through-space interproton connectivities between anthramycin H13 and $^{11}AH_2$ (A), anthramycin H12 and H13 (B), anthramycin H6 and H7 (C), and anthramycin H11 and ^{4}CH1′ (D), and H5 and H6 connectivities for ^{4}C and ^{10}C (E and F, respectively).

C12 and C13 was also evident. The corresponding scalar couplings between H12 and H13 were found in the COSY spectrum (Figure 5). Confirmation of the NOE between the $^{11}AH_2$ proton and the H13 proton of anthramycin observed in Figure 6 was obtained through a one-dimensional NOE difference experiment (Figure 7A). The critical assignment of the $^{11}AH_2$ proton was also confirmed by a one-dimensional NOE difference experiment (Figure 7B). The lower T_1 relaxation time (3.38 s) of the $^{11}AH_2$ proton (Table IA) relative to other adenine H_2 protons (4.96–5.46 s) in anthramycin–d(ATGCAT)$_2$ is also in accord with its close proximity to an anthramycin proton. Significantly, examination of the NOESY spectrum in the region where a cross-peak between the anthramycin 8-CH_3 and $^{11}AH_2$ would be expected did not show evidence of a through-space interproton drug–nucleotide connectivity (unpublished results). Additional through-space interproton connectivities between anthramycin protons at C1a and C1b and the $^{11}AH_2$ proton were also identified (unpublished results). These interproton connectivities are only consistent with the 3′-oriented species (i.e., **A** and **B** in Figure 3).

In a previous two-dimensional ^{1}H NMR study on the anthramycin–d(ATGCAT)$_2$ adduct, an NOE cross-peak between the aromatic 8-CH_3 protons of anthramycin and the $^5AH_2$ was tentatively identified[18a] to support assignment of species **A** in Figure 3 as the anthramycin–d(ATGCAT)$_2$ adduct. Consequently, we

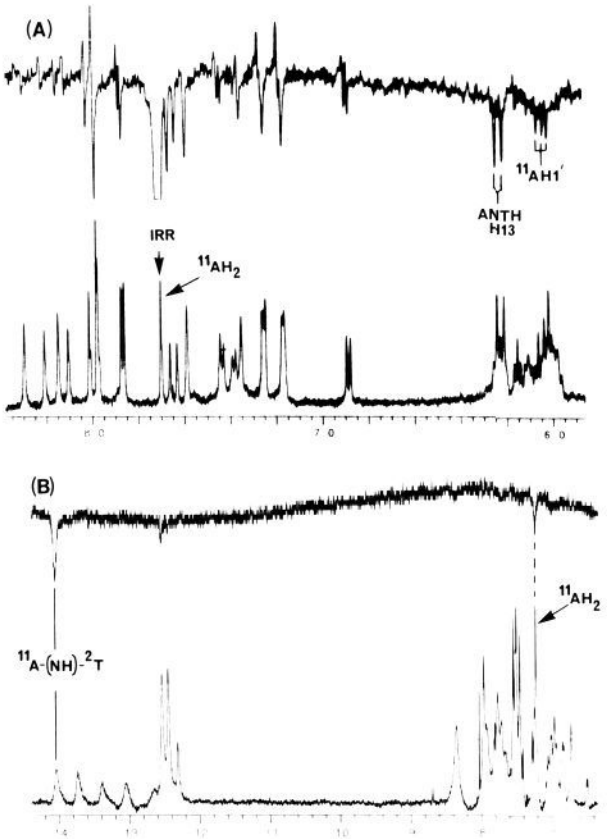

Figure 7. One-dimensional NOE difference spectra obtained by irradiation on the $^{11}AH_2$ at 23 °C (A) and ^{11}A(NH)^{2}T at 5 °C (B) protons to confirm the NOE cross-peak observed in Figure 6 and the assignment of the $^{11}AH_2$ proton, respectively.

examined the NOESY spectra in the regions corresponding to the expected positions for an NOE cross-peak between the anthramycin 8-CH_3 protons and $^5AH_2$ proton. An appropriate cross-peak was not evident in our two-dimensional NOE experiments, which would confirm these connectivities (unpublished results). In addition, irradiation on the $^5AH_2$ proton did not show a NOE into the anthramycin 8-CH_3 protons (unpublished results). We were puzzled why we were unable to reproduce the cross-peak for the proton connectivities between $^5AH_2$ and anthramycin 8-CH_3. Therefore, molecular modeling was used to determine the critical drug–nucleotide interproton distances in species **A** of Figure 3. Of these computed drug–nucleotide interproton distances

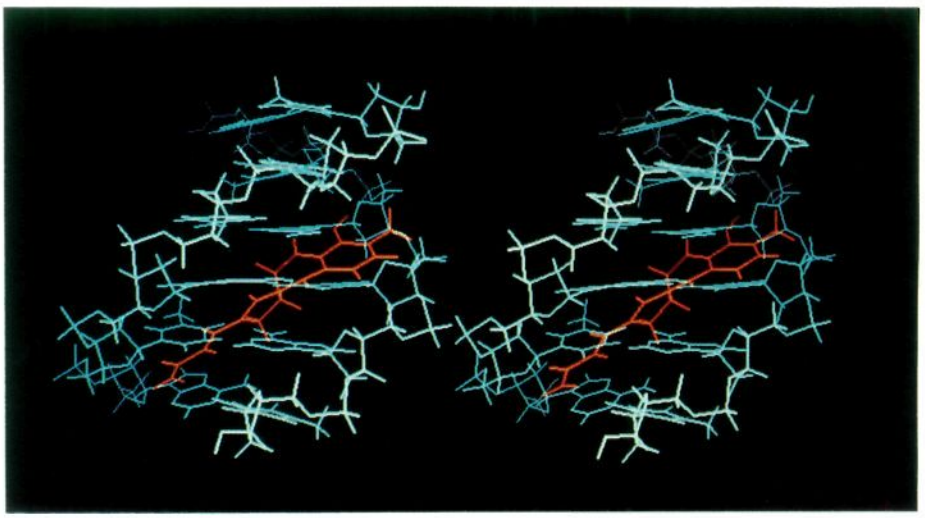

Figure 8. Stereodrawings of the anthramycin–d(ATGCAT)$_2$ (Figure 3A) energy minimized by AMBER.

Table III. Energies (kcal/mol) of Covalent Complexes between Anthramycin and d(ATGCAT)$_2$[a]

species	total	intermolecular			distortion[b]			net binding[c]
		steric	elstat	total	drug	DNA	total	
A (11S, 3′)	-391.8	-33.5	-26.2	-59.7	2.4	16.0	18.4	-41.3
B (11R, 3′)	-372.6	-25.2	-19.6	-44.8	6.3	16.4	22.7	-22.1
C (11S, 5′)	-385.4	-29.7	-21.0	-50.7	2.7	12.6	15.3	-35.4
D (11R, 5′)	-385.4	-32.2	-18.0	-50.2	2.0	13.3	15.3	-34.9

[a] These energies are valid only for comparison within the table. They should not be compared with other drugs or other DNA segments. [b] Drug distortion and helix distortion energies equal their values in the complex less their values when minimized alone (14.0 and -364.4 kcal/mol, respectively). [c] Net binding energy equals the total intermolecular binding minus the total distortion energy.

Table IV. Energies (kcal/mol) for the Interactions of Anthramycin with Individual Residues of d(ATGCAT)$_2$[a]

residue		species[b]			
		A	B	C	D
3	S		-3.1		
3	G			-8.2	-5.9
3, 4	P	-8.7	-3.3		
4	C	-5.4*	-4.1*		
5	S	-3.3			
5	A	-3.3		-8.6*	-8.7*
10	C		-3.3	-3.2	-3.2
11	S			-3.4	
11	A			-4.2	-3.5
12	S			-3.2	-3.7
12	T	-6.7*	-6.5*		

[a] Only energies >-3.0 kcal/mol are listed. [b] S stands for sugar. Asterisk identifies an interaction involving a hydrogen bond (see Table V). The hydrogen bond between HN2B of ^{9}G and O9 of anthramycin in species A has an energy of only -2.7 kcal/mol.

(6.1–6.2 Å for 8-CH$_3$ to ^{5}AH$_2$ and 2.4–2.5 Å for H13 to ^{11}AH$_2$), *only* the anthramycin H13 to ^{11}AH$_2$ interproton distance would be expected to be close enough to allow observation of an NOE cross-peak.[21] Therefore, the results reported here provide unequivocal evidence for the orientation of the anthramycin molecule in the minor groove of DNA.

Assignment of the Covalent Linkage Site Geometry in Anthramycin-d(ATGCAT)$_2$ by ^{1}H NMR. On the basis of the observed two-dimensional NOE through-space connectivity between the ^{11}AH$_2$ proton and the anthramycin H13 proton, only species **A** and **B** in Figure 3 are possible. These species differ in the stereochemistry at the covalent linkage site (**A**, 11*S*; **B**, 11*R*). CPK model building studies,[8] previous molecular modeling,[13-15] and the results of molecular modeling described later predict that the 11*S* geometry at the covalent linkage site is that favored for bonding of anthramycin to DNA. In anthramycin 11-methyl ether, of the two possible diastereomers (11*S*,11a*S* and 11*R*,11a*S*) only the 11*S*,11a*S* can give rise to a one-bond scalar coupling pattern, since the 11*R*,11a*S* diastereomer of anthramycin has a predicted 77.6° dihedral angle between the protons at C11 and C11a and consequently is shown to lack a significant observable coupling.[4] The two-dimensional COSY spectrum of anthramycin-d(ATGCAT)$_2$ shows a strong cross-peak between a proton at 6.03 ppm and a doublet at 4.45 ppm identified as the C11 and C11a protons of anthramycin, respectively (Figure 5). This seemingly provides confirmation that the geometry at the covalent linkage site is 11*S* as previously predicted, first by CPK models[8] and then by computational methods reported previously.[13-15] However, upon energy minimization of the anthramycin-d(ATGCAT)$_2$ adducts with the 11*S* and 11*R* configurations (**A** and **B** in Figure 3) the H11-C11-C11a-H11a dihedral angles are 172° (11*S*) and 17.4° (11*R*). Therefore, due to the apparent considerable flexibility in the drug molecule, the seven-membered ring may adopt a conformation that accommodates to the local constraints within the minor groove of DNA. Consequently, it is apparently more difficult to differentiate, by ^{1}H NMR examination of the scalar coupling between H11 and H11a, between the 11*S* and 11*R* configurations in anthramycin-d(ATGCAT)$_2$. Therefore, while the two-dimensional NOE data of Figure 6 can narrow down the four possibilities in Figure 3 to either **A** or **B**, the COSY data alone cannot definitively differentiate between these remaining species.

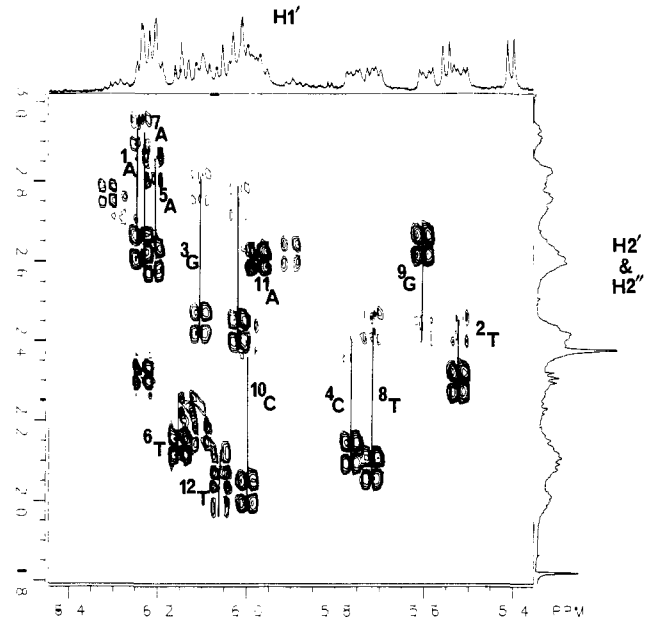

Figure 9. Two-dimensional expansion of a region of the COSY spectrum that shows coupling of the H1′ protons into the H2′ and H2″ protons. The H2″ protons are downfield of the H2′ protons.

Since the scalar coupling between protons at C11 and C11a did not provide a definitive answer for the stereochemistry at the covalent linkage site, alternative ^{1}H NMR evidence was sought. One possible solution would be to identify one or more through-space intermolecular proton–proton couplings that would *only* be consistent with either species **A** (11*S*, 3′-orientation) or species **B** (11*R*, 3′-orientation). In addition to the previously described anthramycin H13 to ^{11}AH$_2$ interproton connectivity, three other drug–nucleotide interproton connectivities were identified, i.e., anthramycin H1a and H1b to ^{11}AH$_2$ (unpublished results) and anthramycin H11 to ^{4}CH1′. Of these NOEs, the anthramycin H11 to ^{4}CH1′ is particularly strong (**D** in Figure 6) as compared to cross-peaks C, E, and F in Figure 6. An analysis of the calculated distances between each pair of protons for the energy-minimized species **A** and **B** reveals that the anthramycin interproton distances to ^{11}AH$_2$ are not useful in differentiating between these possibilities. However, the very strong NOE between H11 of anthramycin and the ^{4}CH1′ is more consistent with the 2.88-Å distance for species **A** than the 3.60-Å distance for species **B**.

In addition to intermolecular proton distances that would potentially differentiate between species **A** and **B** in Figure 3, it also seemed possible that the different environments of the 11*S* or 11*R* protons in species **A** and **B** might provide a further piece of independent evidence to support one species over the other. In fact, in related studies[17] with tomaymycin covalently bound to d(CICGAATTCICG)$_2$ it has been demonstrated that the 11*S*,11a*S* species having a 3′-orientation is associated with a large downfield shift (0.9 ppm) of the C11 proton. An equivalent C11 proton in just one species of the tomaymycin-d(ATGCAT)$_2$ adduct also

(21) Although under our experimental conditions we were unable to detect this NOE connectivity, the authors of ref 18a report they consistently show a weak, but observable, connectivity for 8-CH$_3$ to ^{5}AH$_2$ at 600-ms mixing time in the two-dimensional NOESY and the one-dimensional NOE difference experiment: Krugh, T. R. Private communication.

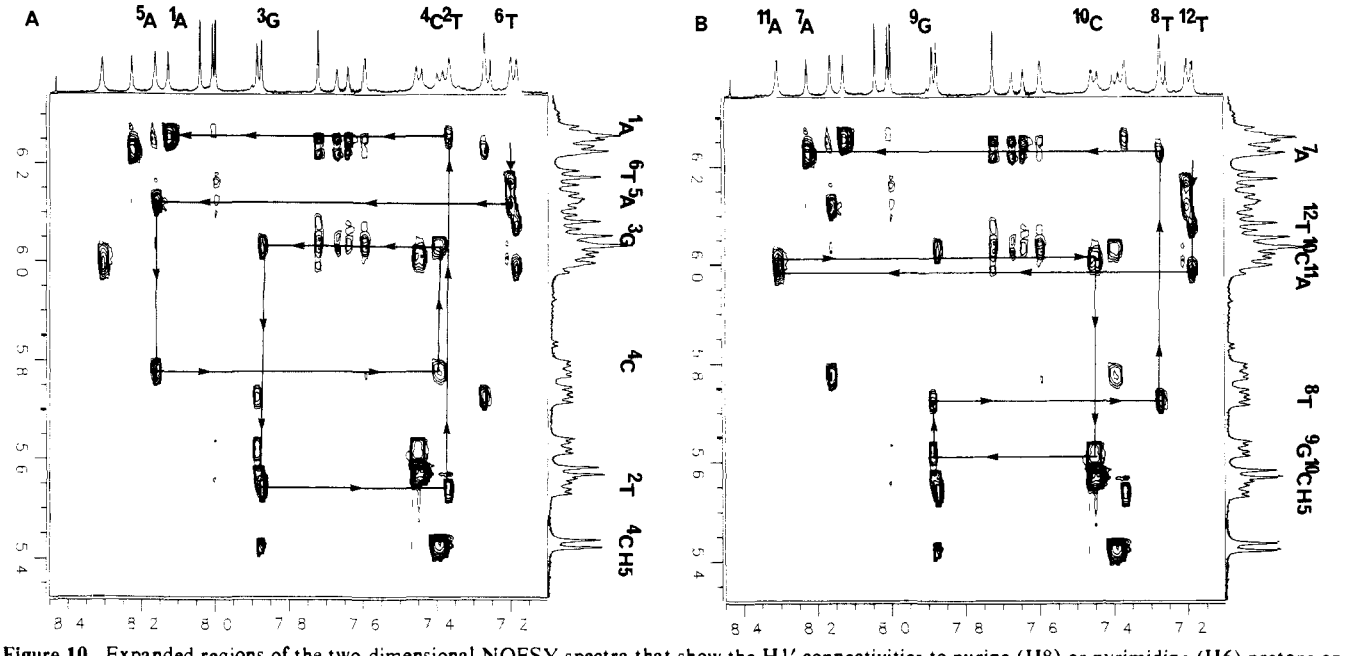

Figure 10. Expanded regions of the two-dimensional NOESY spectra that show the H1′ connectivities to purine (H8) or pyrimidine (H6) protons on the covalently (A) and noncovalently (B) modified strands.

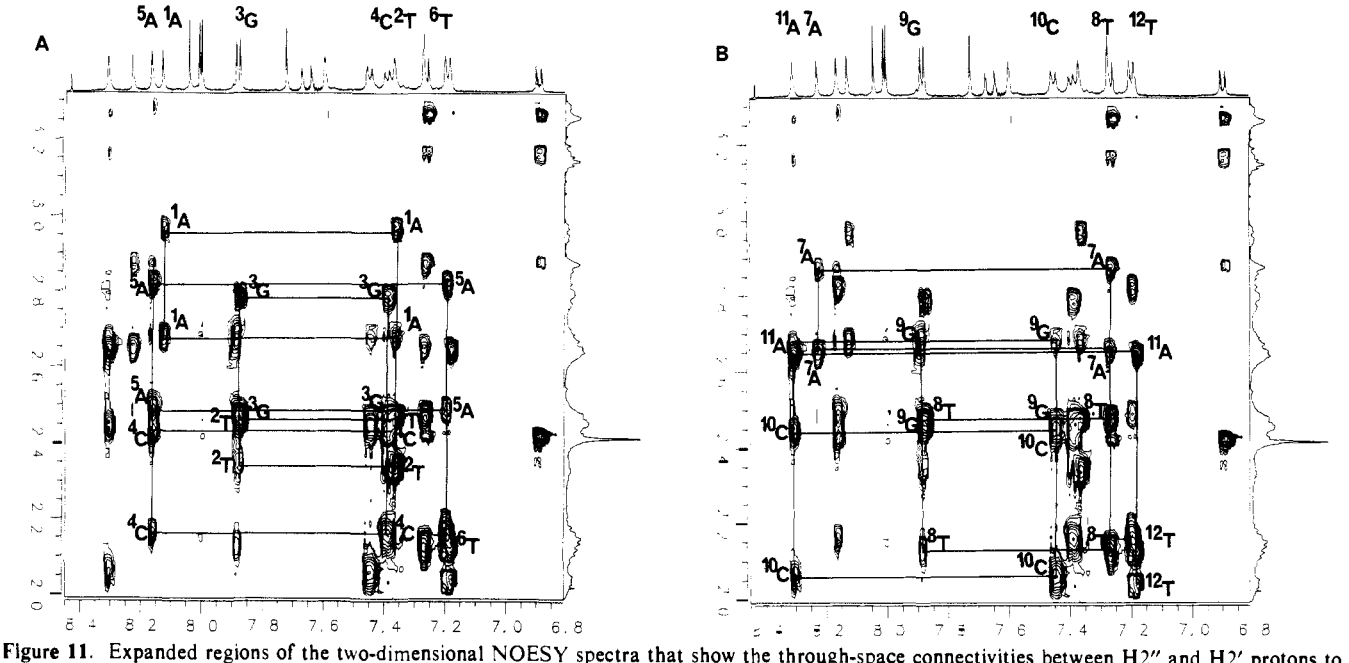

Figure 11. Expanded regions of the two-dimensional NOESY spectra that show the through-space connectivities between H2″ and H2′ protons to purine (H8) or pyrimidine (H6) protons on the covalently (A) and noncovalently (B) modified strands.

shows this characteristic large downfield chemical shift. Since in the anthramycin–d(ATGCAT)$_2$ duplex the anthramycin H11 undergoes a downfield shift of about the same magnitude (1.04 ppm), this provides further support that the species of anthramycin bound to d(ATGCAT)$_2$ is the 11*S*, 3′-oriented adduct.

Prediction of the Preferred Bonding Orientation and Covalent Linkage Stereochemistry of Anthramycin on d(ATGCAT)$_2$ by Molecular Modeling. Anthramycin was covalently bound through its C11 atom to the exocyclic 2-amino group (N-2) of ^{3}G in d(ATGCAT)$_2$. Four different binding modes were modeled: the *R* and *S* configurations at C11 of anthramycin, each with the drug positioned in the minor groove so that its aromatic ring was pointing toward the 3′- or the 5′-end of the covalently bound strand of d(ATGCAT)$_2$. Following energy minimization in AMBER, the net binding energy for each species was calculated from its total intermolecular drug-DNA binding energy minus the helix and drug distortion energies that resulted from the induced fit (Table III). There was a clear preference by 5.9 kcal/mol for the covalent complex with 11*S* configuration and aromatic ring toward the 3′-direction (Figure 8). This result agrees with the direction of groove binding found in an earlier study that used the united-atom model for anthramycin and d(ATGCAT)$_2$ and had no specification of configuration at C11.[14] The earlier model adopted the 11*S* configuration in the course of energy refinement. More significantly there is a 19.2 kcal/mol difference in net binding energies between species A and B of Figure 3. This clearly differentiates between the two viable alternatives (A and B) remaining after determination of the orientation of anthramycin in the minor groove of d(ATGCAT)$_2$ (see earlier text) in favor of species A, which has the 11*S* stereochemistry and the aromatic ring oriented to the 3′-side. So while no single experimental or theoretical result is definitive in differentiating between species A and B in Figure 3, each piece of evidence (NOESY, chemical shift change of C11, and molecular modeling) when considered together provides a level of high confidence in predicting species A as the species found in solution.

The explanation for the greater stability of the 11*S*, 3′-direction complex over the next two favored complexes lies not in lower helix

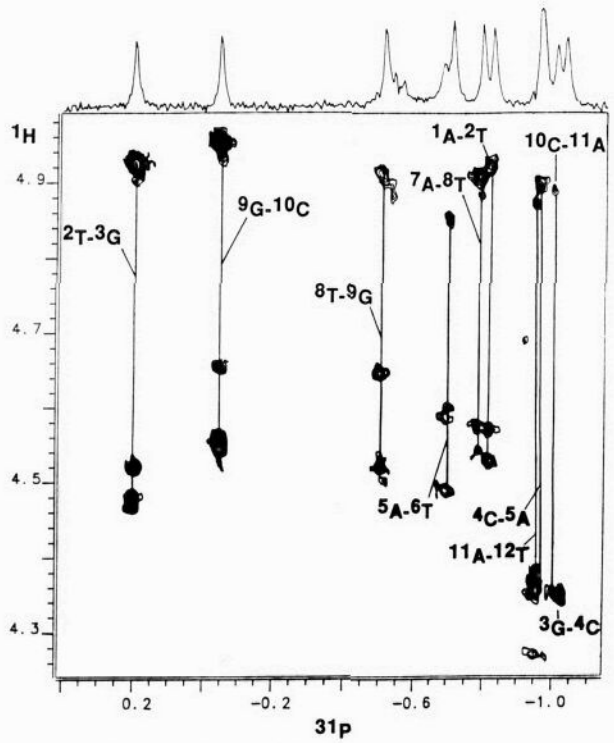

Figure 12. Two-dimensional ^1H–^{31}P *J*-correlated NMR spectrum of the anthramycin–d(ATGCAT)$_2$ adduct.

distortion energy but in greater intermolecular binding, as shown in Table III. This intermolecular binding is divided into the interactions between anthramycin and individual residues of d-(ATGCAT)$_2$ in Table IV. Among these interactions, hydrogen bond formation is especially significant. Table V lists the hydrogen bonds in the four different complexes, and Table IV indicates how they affect the intermolecular binding energies. The 11*S*, 3′-direction complex has the most hydrogen bonds, three, although one of them has less than −3.0 kcal/mol energy. There are two hydrogen bonds for the 11*R*, 3′-direction complex, but it suffers from serious distortion, especially in the drug, and poor overall

Table V. Hydrogen Bond Parameters for Anthramycin–d(ATGCAT)$_2$ Interactions[a]

species	hydrogen atom	acceptor atom	length (Å)	angle (deg)
A (11*S*, 3′)	HN2B (^{9}G)	09 (ANTH)	1.83	141.4
	HN10 (ANTH)	02 (^{4}C)	1.99	133.0
	HN14A (ANTH)[b]	02 (^{12}T)	1.88	149.0
B (11*R*, 3′)	HN10 (ANTH)	02 (^{4}C)	2.22	116.4
	HN14A (ANTH)	02 (^{12}T)	1.83	159.3
C (11*S*, 5′)	HN14A (ANTH)	N3 (^{5}A)	1.85	165.2
D (11*R*, 5′)	HN14A (ANTH)	N3 (^{5}A)	1.88	168.5

[a] Only bond lengths <2.5 Å are listed. [b] Anthramycin = ANTH. HN14A is the upper hydrogen on the amide nitrogen as it appears in Figure 1.

intermolecular binding. The other two complexes have only one hydrogen bond each. One of the main sources of helix distortion energy in the four complexes is a loss of about 6–8 kcal/mol in the interactions between the covalently bound guanine and its opposing cytosine (^{3}G–^{10}C). There are no other significant changes in these Watson–Crick base-pairing energies or in the stacking energies between bases. The remainder of the helix distortion energies are distribution throughout the system so that there are many small local distortions.

In a previous combined fluorescence, ^1H NMR, and molecular modeling study,[16] we have shown that there are two species of tomaymycin–d(ATGCAT)$_2$ adducts present in approximately equal amounts. These differ in their linkage site geometries and are most likely equivalent to species **A** and **D** of Figure 3. The results reported here strongly imply that just species **A** is present in anthramycin–d(ATGCAT)$_2$. While an exact energy difference between two species such as **A** and **D**, which would predict the presence of only one species rather than two, is not known, it is reassuring to note that while there is an energy difference of 6.4 kcal/mol between species **A** and **D** for anthramycin–d-(ATGCAT)$_2$, there is only a 4.0 kcal/mol difference between species **A** and **D** for tomaymycin–d(ATGCAT)$_2$.[16] Further examples will, however, be required before the predictability of molecular mechanics can be relied upon for these types of predictions.

Determination of the Effect of Anthramycin Bonding on Local DNA Structure by Two-Dimensional ^{31}P and ^1H NMR. Previous studies on anthramycin–DNA adducts with enzymatic (S_1-nuclease) and chemical (BND–cellulose chromatography) probes

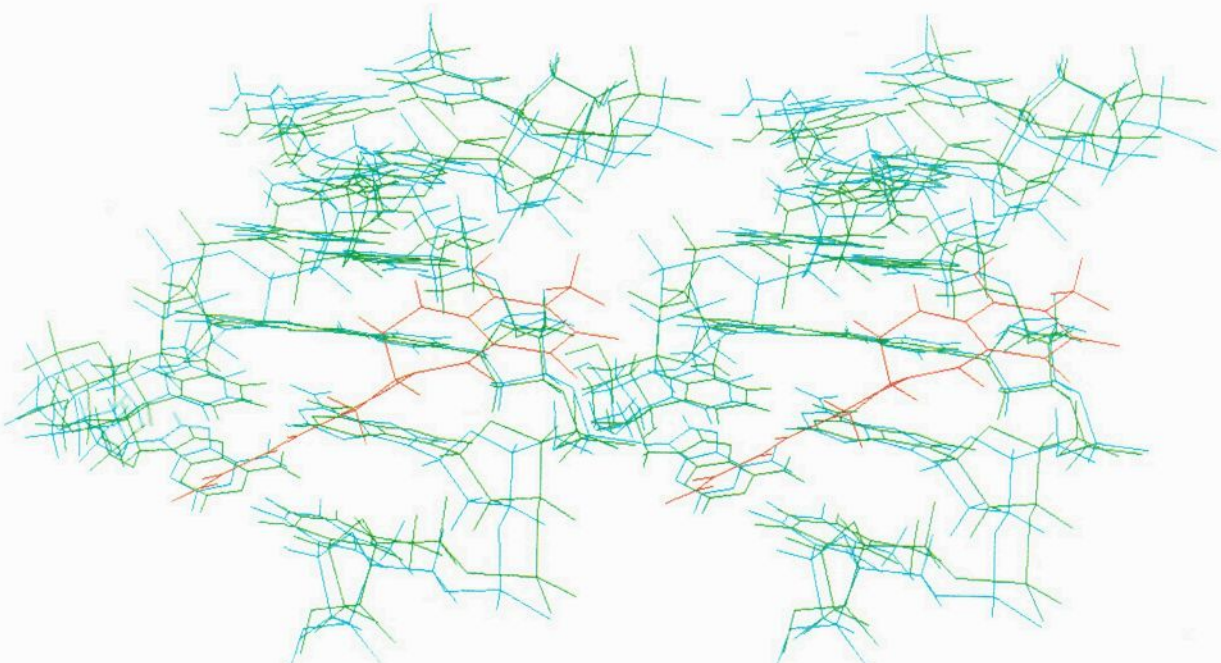

Figure 13. Stereodrawings of the superimposed d(ATGCAT)$_2$ in orange and anthramycin–d(ATGCAT)$_2$ in magenta and yellow.

have suggested that drug bonding causes little distortion of local DNA structure.[8] A more recent high-resolution gel electrophoresis study with use of (methidium-propyl)EDTA–Fe(II) and methylene blue to determine the sequence specificity of anthramycin and related P[1,4]Bs showed that there are drug-induced changes in DNA structure and/or dynamics that can be detected with these reagents.[11] In vivo studies in repair-proficient and -deficient human fibroblast cell lines demonstrate that the excision repair system, usually associated with bulky and distortive DNA adducts, recognizes and removes up to 50% of the anthramycin–DNA adducts during a 72-h period. Previous modeling studies with the molecular mechanics program AMBER[14,15] predict little change in local DNA structure, while the SIR program predicts a change to an A-type DNA structure with a negative tilt of base pairs and opening of the minor groove of DNA. In view of these inconsistencies between theoretical studies[13-15] and the, perhaps, surprising ability of the excision pair system in human cells to recognize a nondistortive and uncharged DNA adduct,[7] it was important to determine how drug bonding affects local DNA structure.

The three-dimensional structure of drug-modified oligomers such as the anthramycin–d(ATGCAT)$_2$ duplex is fixed by the sugar geometry, the glycosidic bond rotation, and the conformation of the sugar–phosphate backbone. Two-dimensional ^{1}H NMR techniques including COSY and NOESY experiments can be used to distinguish between the various families of DNA structure such as A, B, and Z. However, this strategy requires that assignments for aromatic, H1′, H2′, H2″, H3′, and H4′ protons be unequivocally made for each nucleotide. We have used the standard approaches for these assignments, which depends upon sequential imino, aromatic, and sugar assignments for each individual base–sugar set. Imino and aromatic protons for anthramycin–d(ATGCAT)$_2$ adduct have been assigned previously by melting experiments and one-dimensional NOE difference spectra.[18a] These assignments were confirmed in this study (unpublished results). On the basis of an unequivocal assignment of the guanine NH proton at the covalent linkage site in a tomaymycin–12-*mer* duplex adduct[17] at 8.9 ppm, we tentatively assign the broad resonance as 8.4 ppm (Figure 7B) in part to this same proton.

A. Effect of Anthramycin Bonding on Sugar Geometries in d(ATGCAT)$_2$. The vicinal coupling constants among sugar protons vary as a function of pseudorotation angle.[22] While the coupling constants for H2′ to H3′ and H1′ to H2″ are relatively insensitive to sugar pucker, the H1′ to H2′, H3′ to H4′, and H2″ to H3′ show considerable variation. B-Type DNA exists predominantly in a C2′-endo sugar conformation, which is characterized by a large H1′ to H2′ coupling and the absence of significant H2″ to H3′ and H3′ to H4′ couplings. In contrast, an A-type DNA conformation largely maintains a C3′-endo conformation characterized by a large H2″ to H3′ and H3′ to H4′ couplings but lacks significant H1′ to H2′ coupling.

The two-dimensional COSY expansion of the region showing the H1′ to H2″ and H2′ and the H3′ to H2″ and H2′ couplings is shown in Figure 9. The H2″ signals are downfield of the H2′ signals, except in the case of ^{9}G.[23] For all of the H1′ to H2″ and H2′ couplings, except those associated with ^{9}G, the cross-peaks to H2′ are more intense than the cross-peaks to H2″. The coincidence of the H2″ and H2′ resonance signals for ^{5}A and ^{12}T does not permit comparison of their relative intensities. These data are consistent with a C2′-endo conformation for the remainder of the nucleotides. Weak cross-peaks between H3′ and H4′ and H2″ to H3′ (unpublished results) are also in accord with a C2′-endo conformation for these sugars. The results of the COSY experiments indicate that most of the sugars in the anthramycin–d(ATGCAT)$_2$ adduct maintain the C2′-endo geometry associated with B-type DNA, which is also found in d(ATGCAT) alone.

B. Effect of Anthramycin Bonding on Glycosidic Dihedral Angles in d(ATGCAT)$_2$. The relative intensities of the intra- and internucleotide connectivities between H1′ and H6 or H8 protons and H2′ to H6 or H8 protons provide important information on the glycosidic dihedral angle and indirect information on the sugar phosphate backbone geometry. For example, while B-type DNA shows shorter intranucleotide H2′ to H6 or H8 connectivities than 3′ to 5′ internucleotide H2′ to H6 of H8 connectivities, the reverse is true for A-type DNA.

Expanded regions of the two-dimensional NOESY spectra showing H1′ connectivities to purine H8 or pyrimidine H6 protons are shown in Figure 10A,B. On both the covalently (^{1}A to ^{6}T) and the noncovalently (^{7}A to ^{12}T) modified strands, complete 3′ to 5′ sequential "walks" between the internucleotide connectivity for H1′ of ^{6}T (or ^{12}T) and H8 of ^{5}A (or ^{11}A) to the intranucleotide H1′ to H8 of ^{1}A (or ^{7}A) can be made. Of these connectivities only the ^{10}C intranucleotide cross-peak may be somewhat less intense than the other intranucleotide cross-peaks. This is also true of the d(ATGCAT). No significant changes in intensities of internucleotide cross-peaks are observed.

B-Type (C2′-endo) and A-type (C3′-endo) DNA conformations can be differentiated by H6 (H8) connectivities to H2′ protons. For C2′-endo sugar pucker the intranucleotide connectivity (H8/H6 to H2′) is more intense than to the 5′ neighboring H2′. The reverse is true for C3′-endo or A-type helicies.[24] The H2″ and H2′ through-space connectivities to the purine H8's and pyrimidine H6's are shown in Figure 11A,B. In this particular experiment the long mixing time (500 ms) permitted us to observe not only connectivities between the H2′ to aromatic proton via intra- and internucleotide pathways but also H2″ connectivities to the aromatic protons. For example, at 7.25 ppm we observe four connectivities for the H6 proton of ^{2}T. These are from downfield to upfield, the internucleotide ^{1}AH2″ to ^{2}TH6 AH2′ to ^{2}TH6 and the intranucleotide ^{2}TH2″ to ^{2}TH6 and 2TH2′ to 2TH6 connectivities for this pair of nucleotides. For both the covalently and noncovalently modified strands (Figure 12A,B) the pattern of stronger intra- vs internucleotide connectivities for the aromatic to H2′ and H2″ proton pairs holds at shorter mixing times. This confirms C2′-endo or B-type conformation for both strands. In some cases overlapping cross-peaks (i.e., ^{3}G and ^{9}G) do not permit comparison.

C. Effect of Anthramycin Bonding on Phosphate Backbone Conformation. A comparison of the ^{31}P NMR spectra for d(ATGCAT) and the anthramycin–d(ATGCAT)$_2$ adduct (Figure 3) revealed a significant downfield shift for two of the ^{31}P NMR signals in the duplex adduct. In order to determine the identity of these downfield-shifted phosphates, d(ATGCAT) was prepared containing specifically ^{17}O-labeled phosphates. The observed broadening of certain ^{31}P resonances in spectra of both the d(ATGCAT) and the anthramycin adduct is due to the quadrupolar nature of an attached ^{17}O nucleus. This permits assignment of ^{31}P resonances to pairs of phosphates in the anthramycin–d(ATGCAT)$_2$ adduct. In this way, the two downfield-shifted ^{31}P resonances at +0.20 and −0.04 ppm (Figure 3) of the anthramycin–d(ATGCAT)$_2$ adduct can be assigned to phosphates for T-G and G-C (5′ to 3′) steps, respectively (unpublished results). Because the anthramycin–d(ATGCAT)$_2$ adduct possesses nonsymmetrical but self-complementary strands, corresponding upfield

(22) Chary, K. V. R.; Hosur, R. V.; Govil, G.; Zu-kun, T.; Miles, H. T. *Biochemistry* **1987**, *26*, 1315. Altona, C.; Sundaralingam, M. *J. Am. Chem. Soc.* **1972**, *94*, 8205.

(23) It is generally observed that H2′ protons resonate upfield of their intranucleotide H2″ protons and that the former are spatially closer to their intranucleotide purine H8 or pyrimidine H6 base protons. Cross-peak intensities in the two-dimensional NOESY at a short mixing time (100 ms) and a one-dimensional NOE difference experiment, in which the ^{9}G H8 proton was irradiated and the intranucleotide sugar protons were observed, indicate that the ^{9}G H2″ proton resonates upfield (2.47 ppm) of the ^{9}G H2′ proton (2.70 ppm; Table 1B). This is confirmed by cross-peak intensities between H1′ with H2′ and H2″ (unpublished results), where H1′ is predicted to be closer to H2″ (2.3 Å) than to H2′ (3.0 Å): Van De Ven, F. J. M.; Hilbers, C. W. *Eur. J. Biochem.* **1988**, *178*, 1. Predictions from AMBER suggest that the sugar conformation of ^{9}G might be O1′-exo in the d(ATGCAT)$_2$–anthramycin adduct. Distances derived from this modeling are not significantly different from those predicted for C2′-endo sugars: ^{9}G H8–H2′, 2.3 Å; ^{9}G H8–H2″, 3.63 Å; ^{9}G H1′–H2′, 3.06 Å; ^{9}G H1′–H2″, 2.47 Å. As such, NOE intensities alone cannot discriminate between typical C2′-endo and O1′-exo averaged sugar geometries. However, on the basis of the observed coupling between ^{9}G H1′ and the downfield resonance designated as H2′ (Table 1B, Figure 9), we conclude that the sugar geometry at ^{9}G is C2′-endo.

(24) Haasnoot, C. A. G.; Westerink, H. P.; van der Marel, G. A.; van Boom, J. H. *J. Biomol. Struct. Dyn.* **1984**, *2*, 345.

^{31}P resonances at −0.51 and −1.02 ppm for T-G and G-C (5′ to 3′) steps were also identified. A two-dimensional ^{31}P–^{1}H *J*-correlation NMR experiment (Figure 12), in combination with previously assigned H3′, H4′, and H5′ protons, allowed assignments of the ^{17}O-broadened ^{31}P resonances to either the covalently or noncovalently modified strands. The two furthermost downfield-shifted ^{31}P resonances were thus identified as those 5′- to 3′-steps between ^{2}T-^{3}G and ^{9}G-^{10}C, on the covalently and noncovalently modified strands, respectively.

It is perhaps not surprising that one of the downfield-shifted ^{31}P NMR signals (^{2}T-^{3}G) is directly adjacent to the covalent modification site on d(ATGCAT)$_2$. A similar observation has been made for the phosphate between 5′-(C-G) contained in the sequence 5′-CGA-3′ upon bonding of tomaymycin.[17] In this case, examination of the ^{1}H NMR spectra allowed us to associate this downfield ^{31}P resonance to a perturbation of backbone confirmation. The second downfield-shifted ^{31}P resonance in the anthramycin–d(ATCGAT)$_2$ adduct is between the C and G (5′–3′) on the noncovalently modified strand. This is directly adjacent to ^{9}G, which shows the upfield shift of the H2″ proton. In the bis(tomaymycin)–12-*mer* adduct where the bonding sequence is 5′-CGA-3′, an equivalent downfield-shifted ^{31}P resonance on the noncovalently modified strand does not occur. Anthramycin is bound in a least favored sequence (5′-TGC=5′-PyGPy), and tomaymycin is bound in a more favored sequence (5′-CGA= 5′-PyGPu). The extra downfield-shifted ^{31}P resonance in 5′-TGC may be the result of deshielding by anthramycin. Alternatively, the ^{31}P shifts may be an indication of perturbation of DNA structure, which could be required for covalent bonding of anthramycin to this sequence. Furthermore, this could be the reason that PyGPy sequences are less favored bonding sequences for P[1,4]Bs than PyGPu sequences.[11] This idea is further supported by unpublished ^{31}P NMR studies on anthramycin bound to an oligomer containing the covalent bonding sequence 5′–AGA–3′. In this case downfield-shifted ^{31}P resonance signals are not observed. Since this oligomer belongs to the most favored 5′-PuGPu sequence, ^{31}P NMR may be a sensitive tool to evaluate backbone distortion of DNA, as this relates to P[1,4]B preferred sequence selectivity.[25]

Comparison of Experimental (NMR) and Molecular Modeling Results. There is generally excellent agreement between the experimental (NMR) findings reported here and the predictions from the molecular mechanics program AMBER. For example, the AMBER prediction of species A (Figure 3) as the species found in solution is in accord with the experimental results. AMBER also is predictive of the relatively nondistortive nature of the anthramycin–d(ATGCAT)$_2$ (Figure 13). Molecular modeling of species A (Figure 3) predicts a narrower groove width for the duplex adduct than in the duplex alone. In the structure of this duplex, built in AMBER from Arnott's B DNA geometry and minimized, the distances between A5-H2 and G9-H1′ and between A11-H2 and G3-H1′ are both 4.12 Å. When the drug is covalently bound and the structure is reminimized, the corresponding distances are 3.85 and 3.67 Å, respectively. These indicate a small but definite narrowing of the minor groove. The reason for this behavior, at least according to the models, is found in the hydrogen-bonding pattern between the drug and DNA. Thus, anthramycin is bound covalently, roughly at its center, to one strand and attracted to the opposite strand by hydrogen bonds from each of its ends (HN2B to G9 to O9 of anthramycin and H18A of anthramycin to O2 of T12). These interactions pull the two strands together in the vicinity of the drug. While all these previous modeling studies[13-15] correctly predicted species A (Figure 3) as that species which should be favored, we could find no evidence for the B- to A-type transition predicted by the SIR program.[13]

Conclusions and DNA Repair Implications

(1) Definitive evidence for the orientation of anthramycin bonding in the minor groove of d(ATGCAT)$_2$ (aromatic ring to the 3′-side of ^{3}G) has been obtained by two-dimensional ^{1}H NMR studies.

(2) Combined ^{1}H NMR and molecular modeling results provide strong evidence that in solution anthramycin–d(ATGCAT)$_2$ exists as species **A**. An X-ray structure would be required for unequivocal determination of the stereochemistry at C11 in anthramycin–d(ATGCAT)$_2$.

(3) In contrast to the tomaymycin–d(ATGCAT)$_2$ adducts, which exist, most likely as a 50:50 mixture of species **A** and **D** (Figure 3), the anthramycin–d(ATGCAT)$_2$ adduct exists, at least predominantly, as species **A**.

(4) Anthramycin bonding to d(ATGCAT)$_2$ causes relatively minor distortion of the local DNA structure (Figure 13). The most significant changes are predicted by ^{31}P NMR to occur at the phosphates to the 5′-side of the covalently modified deoxyguanine and to the deoxycytosine on the noncovalently modified strand. The minor-groove width of d(ATGCAT)$_2$ is predicted to be narrower following covalent modification.

(5) Modeling predictions from the molecular mechanics program AMBER are largely confirmed by the ^{1}H NMR studies.

(6) The recognition and repair of nondistortive covalent adducts by DNA repair enzymes is a largely ignored problem. Human fibroblast cells are able to recognize and excise anthramycin–DNA adducts,[7] but these presumably represent a population of adducts in various sequences. It will be important to evaluate the ability of DNA-repair enzymes to recognize and incise anthramycin–DNA adducts of defined structure so that the rules that govern recognition of modified DNA can be extended to nondistortive covalent DNA adducts.

Experimental Procedures

Materials and Preparation. Anthramycin 11-methyl ether (**1b**) was obtained from Hofmann LaRoche. d(ATGCAT) was prepared in house by solid-phase phosphite-triester synthesis[26] and purified across Machery-Nagel Nucleogen HPLC columns with an increasing gradient of sodium chloride in phosphate buffer. ^{17}O-Labeled oligomers were prepared in identical fashion with the exception that 35% isotopically enriched [^{17}O]water (MSD Isotopes) was used in the mixture that oxidizes on intermediate phosphite to a phosphate. The oligomers were desalted across Waters Associates C_{18} Sep-pak cartridges.

An intimate mixture of **1a** and d(ATGCAT) was prepared by adding 3 mg of **1b** in 0.5 mL of HPLC grade methanol to a 23 mM solution of the oligomer in a 10 mM $NaHPO_4$–100 mM NaCl–0.1 mM EDTA buffer adjusted to pH 6.85. The combined solutions were lyophilized to dryness in a Savant Spin Vac concentrator, and the pellet was redissolved in 0.5 mL of Burdick & Jackson HPLC grade H_2O. The resulting solution was heated to 65 °C in a water bath for 20 min and allowed to gradually cool to 4 °C. Excess **1a** and **1b** was removed by purification across C_{18} Sep-pek cartridges. The desalted purified anthramycin–d(ATGCAT)$_2$ duplex adduct was dissolved in 0.6 mL of 10 mM NaOAc–100 mM NaCl–0.1 mM EDTA buffer that had been adjusted to pH 7.2 and lyophilized to dryness followed by lyophilization with 2 × 0.5 mL of D_2O.

NMR Experimental Parameters. All ^{1}H and ^{31}P spectra were collected on the GN-500 NMR spectrometer at the University of Texas at Austin, Austin, TX, at 23 °C, unless otherwise indicated. The NMR samples were prepared in 0.6 mL of D_2O and degassed with argon. Chemical shifts are reported (ppm) with positive values downfield from an external reference of 1 mg/mL TSP in D_2O for ^{1}H and an external reference of 85% H_3PO_4 in D_2O for ^{31}P resonances.

One-dimensional spectra of the exchangeable imino protons and NOE difference spectra were performed on the D_2O sample and the same sample that had been lyophilized and redissolved in 90% H_2O–10% D_2O. Suppression of the H_2O signal was achieved with a 1 3 3 1 pulse sequence,[27] and the protons were irradiated, observed, and assigned at 23, 15, 10, 5, and 0 °C as before.[16] T_1 experiments were performed utilizing the standard nonselective 180°–*T*–90° pulse sequence as before.[16] Ho-

(25) Patel, D. J. *Biochim. Biophys. Acta* **1976**, *442*, 98. Wilson, D. W.; Jones, R. L. *Nucleic Acids Res.* **1982**, *10*, 1399. Marzilli, L. G.; Bannville, D. L.; Zon, G.; Wilson, D. W. *J. Am. Chem. Soc.* **1986**, *108*, 4188. Wilson, D. W.; Jones, R. L. *J. Am. Chem. Soc.* **1986**, *108*, 7113. Gao, X.; Patel, D. J. *Biochemistry* **1988**, *27*, 1744. Gao, X.; Patel, D. J. *Biochemistry* **1989**, *28*, 751.

(26) Atkinson, T.; Smith, M. Solid Phase Synthesis of Oligodeoxyribonucleotides by the Phosphodiester Method. In *Oligonucleotide Synthesis. A Practical Approach*; Gait, M. J., Ed.; TRL: Washington, DC, 1984; pp 35–81.

(27) Hore, P. J. *J. Magn. Reson.* **1983**, *55*, 283.

monuclear scalar coupling was best determined with the standard two-dimensional COSY experiment with 2K complex points in t_2, 1K points in the t_1 domain, and a recycle delay of >2 s in addition to the acquisition time. The two-dimensional phase-sensitive NOESY was acquired with 4K data points in the t_2 dimension, 1K data points in t_1, and a recycle delay of >2 s in addition to the acquisition time.[27,28] Mixing times of 250 and 500 ms were used that were stochastically varied to suppress cross-peaks arising from scalar coupling. A shifted sine bell multiplication apodization of 45% was applied in the t_2 and t_1 domains. ^{1}H-Decoupled ^{31}P spectra were collected at 202.44 MHz, and ^{1}H-^{31}P correlation experiments were performed according to the procedure described by Bax et al.[29]

Molecular Modeling Studies. The crystal structure of **1b** was used as the initial structure in this investigation. Partial atomic charges for anthramycin with the methoxy group removed were provided by Rao et al.[15] Bond length, bond angle, and dihedral parameters for the all atom force field were those presented by Weiner et al.,[31,32] and new parameters specific to anthramycin were given by Rao et al.[15] The resulting structure was minimized with the program AMBER[31] with a distance-dependent dielectric constant, and refinement continued until the rms gradient was less than 0.1 kcal/mol·Å. This minimized structure was docked in the appropriate location and orientations on the hexanucleotide duplex with the aid of the interactive graphics program MIDAS,[33] and then the binding energies were minimized with AMBER and the parameters described above. The helix energy was determined by subtracting the energy of the helix in the anthramycin adduct from that of the separately minimized isolated helix. Distortion energy induced in the anthramycin molecule was determined in the same way.

Structural effects of water and counterions on complexing were neglected in the energy calculations. Although these effects influence the absolute values of binding energies, they should be minimal in comparing relative binding energies wherein the same molecule is used at the same binding site on the duplex.

Acknowledgment. This work was supported by grants from the NIH (GM-22873), National Cancer Institute (R35-CA-49751 and CA-37798), and Welch Foundation. We thank Joann Haddock for her patience in preparing this manuscript. We also thank Shashidhar N. Rao for data on anthramycin and helical distances, Dr. Peter A. Kollman for a copy of AMBER, and Professor Thomas Krugh for unpublished results and useful discussions.

(28) States, D. J.; Habverkorn, R. A.; Ruben, D. J. *J. Magn. Reson.* **1982**, *48*, 286.
(29) Bax, A.; Sarkar, S. K. *J. Magn. Reson.* **1984**, *60*, 170.
(30) Weiner, S. J.; Kollman, P. A.; Case, D.; Singh, U. C.; Ghio, C.; Alagona, G.; Profeta, S., Jr.; Weiner, P. K. *J. Am. Chem. Soc.* **1984**, *106*, 765.
(31) Weiner, S. J.; Kollman, P. A.; Nguyen, D. T.; Case, D. A. *J. Comp. Chem.* **1986**, *7*, 230.
(32) Weiner, P. K.; Kollman, P. A. *J. Comp. Chem.* **1984**, *2*, 287.
(33) Langridge, R.; Ferrin, T. *J. Mol. Graphics* **1984**, *2*, 56.

Resonance Raman Spectra of Reaction Intermediates in the Oxidation Process of Ruthenium(II) and Iron(II) Porphyrins

Insook Rhee Paeng and Kazuo Nakamoto*

Contribution from the Todd Wehr Chemistry Building, Marquette University, Milwaukee, Wisconsin 53233. *Received June 15, 1989*

Abstract: The dioxo ruthenium porphyrins, $RuP(O)_2$ (P = TPP and TMP), were prepared by the oxidation of RuP(CO) with *m*-chloroperoxybenzoic acid (*m*-CPBA). The resonance Raman and IR spectra of $RuP(O)_2$ were measured and their O=Ru=O vibrations including the ^{16}O=Ru=^{18}O and ^{18}O=Ru=^{18}O analogues assigned by normal coordinate calculations. A reaction scheme involving two successive O—O bond cleavages of *m*-CPBA was proposed based on the observed intensity patterns of the O=Ru=O vibrations. When a toluene solution of Ru(TPP) was saturated with O_2 at −80 °C, the ν_s(Ru–O) of (TPP)Ru–O–O–Ru(TPP) was observed at 552 cm^{-1} (533 cm^{-1} for the ^{18}O analogue). Upon raising the temperature, this band disappeared, and the ν_s(O=Ru=O) of Ru(TPP)$(O)_2$ appeared at 811 cm^{-1} (767 cm^{-1} for the ^{18}O analogue). The ν(RuO) of the monoxo complex, O=Ru(TPP), was observed at 780 cm^{-1} when a toluene-d_8 solution of Ru(TPP) was saturated with $^{18}O_2$ at −80 °C. Similar experiments with Ru(OEP) exhibited the ν(RuO) at 820 cm^{-1} (779 cm^{-1} for the ^{18}O analogue). Bands characteristic of the Ru—O—O—Ru bridge and O=Ru=O moiety were not observed for the OEP complex. The six-coordinate, Ru(TPP)(pyridine)O_2 exhibits the ν(Ru—O_2) at 603 cm^{-1}, which is higher than the ν(Fe—O_2) of the corresponding Fe complex (575 cm^{-1}). The resonance Raman spectra of PFe—O—O—FeP and O=FeP (P = TPP, OEP, and other porphyrins), which are formed in the oxidation process of these Fe porphyrins, have been measured including the high-frequency region. In all cases, the peroxo-bridged species and the ferryl species are present at low temperature, and the former is converted into the latter by raising the temperature.

Considerable attention has been given to the interactions between dioxygen and low-valent metalloporphyrins because of their relevance to biological systems. In particular, the reactions of iron porphyrins with dioxygen[1-10] have been studied extensively in the past decade. Recently, the reactions of ruthenium porphyrins with dioxygen have also received considerable attention.

Scheme I

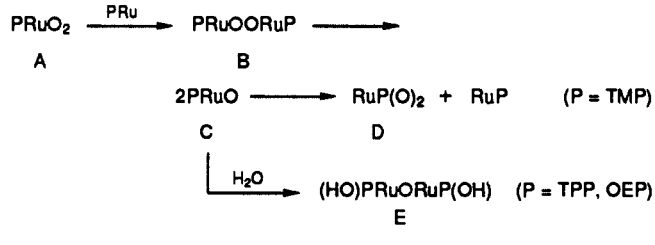

(1) Spiro, T. G. In *Iron Porphyrins*; Lever, A. B. P., Gray, H. B., Eds.; Addison-Wesley; Reading, MA, 1983; Part 2, pp 89-159.
(2) Collman, J. P.; Halbert, T. R.; Suslick, K. S. In *Metal Ion Activation of Dioxygen*; Spiro, T. G., Ed.; Wiley-Interscience, New York, 1980; pp 1-72.
(3) Watanabe, T.; Ama, T.; Nakamoto, K. *J. Phys. Chem.* **1984**, *88*, 440.
(4) Wagner, W.-D.; Paeng, I. R.; Nakamoto, K. *J. Am. Chem. Soc.* **1988**, *110*, 5565.
(5) Bajdor, K.; Nakamoto, K. *J. Am. Chem. Soc.* **1984**, *106*, 3045.
(6) Proniewicz, L. M.; Bajdor, K.; Nakamoto, K. *J. Phys. Chem.* **1986**, *90*, 1560.
(7) Chin, D.-H.; Del Gaudio, J.; La Mar, G. N.; Balch, A. L. *J. Am. Chem. Soc.* **1977**, *99*, 5486.
(8) Chin, D.-H.; La Mar, G. N.; Balch, A. L. *J. Am. Chem. Soc.* **1980**, *102*, 4344.
(9) Latos-Grazynski, L.; Cheng, R.-J.; La Mar, G. N.; Balch, A. L. *J. Am. Chem. Soc.* **1982**, *104*, 5992.

0002-7863/90/1512-3289$02.50/0